THE JOURNAL OF PHYSICAL CHEMISTRY A

Article

Cite This: J. Phys. Chem. A 2019, 123, 4284−4294

pubs.acs.org/JPCA

Coherent State-Based Path Integral Methodology for Computing the Wigner Phase Space Distribution

Published as part of The Journal of Physical Chemistry virtual special issue "Abraham Nitzan Festschrift".

Amartya Bose and Nancy Makri*

Department of Chemistry, University of Illinois, 505 S. Mathews Avenue, Urbana, Illinois 61801, United States

ABSTRACT: The accurate evaluation of the Wigner phase space density for multidimensional system remains a challenging task. Path integral Monte Carlo methods offer a numerically exact approach for obtaining the Boltzmann density in coordinate space, but the Fourier-type integral required to construct the Wigner distribution generally leads to poor convergence. This paper describes a path integral method for constructing the Wigner density which substantially mitigates the Monte Carlo sign problem and thus is applicable to systems with many degrees of freedom. The starting point is the path integral representation of the coherent state density, which does not involve a Fourier integral and thus converges rapidly. We then use the relation between the coherent state and Wigner densities to construct the Wigner function, taking advantage of destructive phase cancellation to truncate the infinite series and thus confine the integrand, avoiding highly oscillatory regions. We also describe the use of information-guided noise reduction (IGNoR) to improve the Monte Carlo statistics in the most challenging regimes. The method is applied to strongly anharmonic one-dimensional models, a system-bath Hamiltonian, as well as the formamide molecule within an *ab initio* quartic potential, and the results are compared to those obtained by various approximate methods. These calculations suggest that the coherent state-based path integral method described in this paper offers an efficient, numerically exact approach for constructing the Wigner phase space density in systems of many degrees of freedom, and thus will be useful for quantizing the initial condition in classical trajectory-based simulations of dynamical properties.

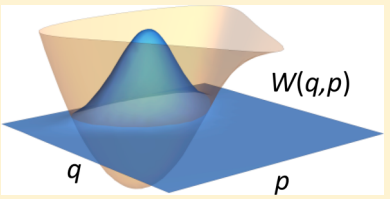

I. INTRODUCTION

Fully quantum mechanical treatments for following the dynamics of condensed phase and biological processes continue to be prohibitively costly in most situations. While some rigorous and accurate methods are currently available for particular types of systems, many simulations continue to rely on classical trajectories. Classical molecular dynamics methods are efficient and robust, and even though they cannot account for quantum mechanical effects, they often lead to usefully accurate predictions. There are several reasons for this success of classical mechanical approximations. One of the hallmarks of quantum mechanics is interference, and this phenomenon tends to be washed out in condensed phase dynamics. Quantum mechanical tunneling is often dominated by over-the-barrier crossing at physiological temperatures. On the other hand, vibrational zero-point energy (ZPE) effects can be significant, as many chemical bonds are relatively cold under common conditions. By design, classical force fields effectively capture some ZPE effects in an average way (although this construction makes them temperature-dependent), but the adequacy of this ZPE treatment is hard to assess. Further, classical force fields are not available for interactions encountered in many materials. A more rigorous but costly approach is force evaluation via *ab initio* electronic structure methods, which produce the Born−Oppenheimer potential surface (and its derivatives). In this case, ZPE effects must be included in the phase space distribution from which classical trajectories are sampled.

There are a few prescriptions for constructing quantum mechanical phase space distributions, of which the most widely used schemes follow the Wigner approach.[1] For a system of one degree of freedom, the Wigner transform of an operator $\hat{O}$ is given by the expression

$$\hat{O}_W(q,p) = \frac{1}{\sqrt{2\pi\hbar}} \int_{-\infty}^{\infty} d\xi \langle q + \frac{1}{2}\xi | \hat{O} | q - \frac{1}{2}\xi \rangle e^{-ip\xi/\hbar} \tag{1.1}$$

The Wigner phase space density is frequently used in connection with the Boltzmann operator, that is, $\hat{O} = Z^{-1}e^{-\beta\hat{H}}$, where $\beta = 1/k_B T$. For simplicity, we denote the thermal Wigner density as $W(q,p)$. The Wigner transform $A_W^\beta(q,p)$ of symmetrically thermalized operators, with $\hat{O} = Z^{-1}\, e^{-\beta\hat{H}/2}\hat{A}e^{-\beta\hat{H}/2}$, is also encountered in the calculation of time correlation functions.

The simplest scheme for approximating dynamical observables in the spirit discussed above is known as the quasiclassical approximation or Wigner dynamics,[1,2] and is equivalent to the linearized semiclassical initial value representation[3−5] (LSC-IVR), which can also be derived from linearizing the path integral expression.[6] According to

Received: January 24, 2019
Revised: April 3, 2019
Published: April 15, 2019

DOI: 10.1021/acs.jpca.9b00758
J. Phys. Chem. A 2019, 123, 4284−4294

this prescription, the time evolution of the expectation value of an operator is given by the integral

$$\langle A(t)\rangle = \int dq_0 \int dp_0 W(q_0, p_0) A(q_t, p_t) \tag{1.2}$$

where q_t, p_t are the phase space coordinates reached by a classical trajectory with initial condition q_0, p_0. Similarly, the choice $\hat{O} = Z^{-1} e^{-\beta\hat{H}}\hat{A}$ yields quasiclassical approximations to time correlation functions. An improved approximation results from the path integral Liouville dynamics[7,8] (PILD) formulation, which by construction rigorously preserves the phase space density.

Further, Wigner phase space distributions are employed in quantum-classical simulations. The mapping Hamiltonian formalism[9−11] replaces the discrete states of a quantum subsystem by continuous degrees of freedom, allowing a unified treatment of all particles by classical trajectories launched from a quantized phase space distribution. Recently, the quantum-classical Liouville equation has been used as the framework for a systematic expansion[12,13] that obtains dynamical information through classical trajectories sampled from the Wigner distribution, retaining the discrete character of the quantum system. A quantum-classical path integral (QCPI) formulation[14−16] has also emerged in the past few years, which allows a rigorous treatment of discrete systems interacting with condensed phase environments the dynamics of which is captured through classical trajectories with Wigner initial conditions.

Unfortunately, the evaluation of the Wigner phase space density in systems of many degrees of freedom is far from straightforward. This is so because the oscillatory phase involved in the Fourier integral leads to a "sign problem", causing exponentially slow convergence of Monte Carlo integration methods. Several approximate treatments have been developed for obtaining the Wigner phase space density. These include local[17] or variationally optimized[6] Gaussian wavepacket approaches, and the thermal Gaussian approximation[18] (which employ frozen Gaussian dynamics[19] in imaginary time), along with extensions that capture quantum corrections.[20] We recently introduced[21,22] a simple, trajectory-based approximate method that makes use of the classical adiabatic theorem to slowly convert the Wigner density of a harmonic reference system to that of the target Hamiltonian. Other recent work[23] has used the quasi-adiabatic propagator path integral methodology[24] to obtain the Wigner distribution of the bath in the case of a system interacting with a bath of independent harmonic oscillators.

An attractive alternative for obtaining a quantized phase space density is offered by the Husimi approach,[25] which is based on the coherent state representation of an operator. The numerical evaluation of the Husimi expression is not as challenging, and several techniques are available for this task, such as semiclassical propagation in imaginary time[26] and numerically exact path integral representations.[27]

In this paper, we introduce a numerically exact path integral method for evaluating the Wigner transform of the Boltzmann operator (or symmetrically thermalized operators). The starting point is the path integral representation of the coherent state distribution, which involves a simple and stable procedure. Subsequently, we use the relation[28] between the Wigner and coherent state densities, which we Taylor-expand. We show that the expansion converges rapidly, and that the omission of high order terms dramatically reduces the instabilities arising from phase cancellation. We also apply the information-guided noise reduction[29] (IGNoR) technique to further improve the statistics of the coherent state-based path integral Wigner (CSPIW) method. In challenging regimes with $\sim 10^3$ variables, we find that the IGNoR processing further reduces the statistical error of the CSPIW results by one or more orders of magnitude.

In section II we derive the CSPIW method for general thermalized quantum mechanical operators. In section III we illustrate the procedure by applying it to one-dimensional model potentials, as well as system-bath Hamiltonians with many degrees of freedom. We also apply the method to an *ab initio* Hamiltonian for the formamide molecule and compare the CSPIW results to those obtained by using the path integral Monte Carlo (PIMC) method. Some concluding remarks are given in section IV.

II. PATH INTEGRAL EXPRESSION OF THE WIGNER DENSITY

a. Direct Path Integral Discretization of the Wigner Integral. In this paper we focus on the Wigner transform of symmetrically thermalized operators,

$$A_W^\beta(q,p) = \frac{1}{\sqrt{2\pi\hbar}} Z^{-1} \int_{-\infty}^{\infty} d\xi e^{-ip\xi/\hbar} \langle q + \tfrac{1}{2}\xi | e^{-\beta\hat{H}/2}\hat{A}\, e^{-\beta\hat{H}/2} | q - \tfrac{1}{2}\xi\rangle \tag{2.1}$$

With a minor modification, the procedure described below may be applied to nonsymmetrically thermalized operators, $Z^{-1} e^{-\beta\hat{H}}\hat{A}$. Throughout this section we use one-dimensional notation for clarity. The extension to systems of many degrees of freedom is straightforward.

Consider first the discretized path integral representation of eq 2.1. We begin by splitting the inverse temperature into $2N$ imaginary time slices of length $\Delta\beta = \beta/2N$ and using the Trotter factorization,[30]

$$e^{-\frac{1}{2}\beta\hat{H}} = (e^{-\frac{1}{2}\Delta\beta\hat{T}}\, e^{-\Delta\beta\hat{V}}\, e^{-\frac{1}{2}\Delta\beta\hat{T}})^N \tag{2.2}$$

where $\hat{T}$ and $\hat{V}$ are the kinetic and potential energy operators, respectively. Inserting the resolution of identity repeatedly, we arrive at the following discretized path integral[31,32] representation of the Wigner transform:

$$\begin{aligned} A_W^\beta(q,p) = \frac{1}{\sqrt{2\pi\hbar}} \int_{-\infty}^{\infty} d\xi \int dx_1 \cdots \int dx_{2N+2} \\ \langle q + \tfrac{1}{2}\xi | e^{-\frac{1}{2}\Delta\beta\hat{T}} | x_1\rangle e^{-\Delta\beta V(x_1)} \langle x_1 | e^{-\Delta\beta\hat{T}} | x_2\rangle \\ e^{-\Delta\beta V(x_2)} \langle x_2 | e^{-\Delta\beta\hat{T}} | x_3\rangle \cdots \langle x_N | e^{-\frac{1}{2}\Delta\beta\hat{T}} | x_{N+1}\rangle \\ \langle x_{N+1} | \hat{A} | x_{N+2}\rangle \langle x_{N+2} | e^{-\frac{1}{2}\Delta\beta\hat{T}} | x_{N+3}\rangle \\ e^{-\Delta\beta V(x_{N+3})} \cdots \langle x_{2N+2} | e^{-\frac{1}{2}\Delta\beta\hat{T}} | q - \tfrac{1}{2}\xi\rangle e^{-ip\xi/\hbar} \end{aligned} \tag{2.3}$$

(Note that a different operator ordering in eq 2.2, with the kinetic energy placed in the middle, would have eliminated two path integral variables. The particular ordering of the Trotter splitting we employ is motivated by the coherent state representation that follows. The choice of ordering in the Trotter factorization does not affect the discussion given below regarding the severity of the sign problem in the numerical evaluation of the Wigner transform.)

The kinetic energy factors in eq 2.3 are given by the usual expression,

DOI: 10.1021/acs.jpca.9b00758
J. Phys. Chem. A 2019, 123, 4284−4294

$$\langle x'|e^{-\Delta\beta\hat{T}}|x''\rangle = \sqrt{\frac{m}{2\pi\hbar^2\Delta\beta}}\, e^{-\frac{m}{2\hbar^2\Delta\beta}(x'-x'')^2} \tag{2.4}$$

This leads to the standard picture, where the path integral variables are thought of as classical "beads", connected via harmonic springs and experiencing an external potential.[33] According to eq 2.4, the dependence on the necklace end points is given by the factor

$$e^{-\frac{m}{\hbar^2\Delta\beta}\left(x_1-q-\frac{1}{2}\xi\right)^2} e^{-\frac{m}{\hbar^2\Delta\beta}\left(x_{2N+2}-q+\frac{1}{2}\xi\right)^2} \tag{2.5}$$

As discussed in the Introduction, the most common use of the Wigner density is in the context of selecting phase space coordinates to be used as initial conditions for classical trajectories, as in eq 1.2. For systems of many degrees of freedom, Monte Carlo methods provide the only viable approach to the required multidimensional integrals. Thus, one needs to identify a sampling function for the phase space variables q and p, the Fourier variable ξ and the path integral beads. The exponential factors in eq 2.3 provide the sampling function for the path integral variables $x_1, \cdots x_{2N+2}$. Further, both the Wigner variable q and the Fourier variable ξ are connected to the first and last beads through eq 2.5, so these variables can also be sampled. According to eq 2.5, $q + \frac{1}{2}\xi$ is held close to x_1, while $q - \frac{1}{2}\xi$ is close to x_{2N+2}. These requirements imply that the magnitude of Fourier variable ξ will be comparable to the distance between the first and last beads. At low temperatures, the open path integral necklace has a large span and its ends are far apart. The resulting large values of the variable ξ lead to a rapidly oscillatory Fourier factor $e^{-ip\xi/\hbar}$, which is likely to cause poor Monte Carlo statistics in systems of many degrees of freedom.

Perhaps an even more bothersome issue with the form of eq 2.3, when used in connection with eq 1.2, is the complete absence of a sampling function for the momentum variable p. Thus, it is clear that the straightforward path integral discretization of the Wigner density is not useful for performing quasiclassical calculations. To remedy this flaw, notice that eq 2.5 is the only part of the path integral expression that is dependent on the difference coordinate ξ, and it has a Gaussian form. Evaluation of the Gaussian integral leads to the result

$$\begin{aligned}&\int d\xi\, e^{-ip\xi/\hbar} e^{-\frac{m}{\hbar^2\Delta\beta}\left(x_1-q-\frac{1}{2}\xi\right)^2} e^{-\frac{m}{\hbar^2\Delta\beta}\left(x_{2N+2}-q+\frac{1}{2}\xi\right)^2}\\ &= \sqrt{\frac{\pi m}{2\hbar^2\Delta\beta}}\, e^{-\frac{2m}{\hbar^2\Delta\beta}\left\{q-\left(\frac{x_1+x_{2N+2}}{2}\right)\right\}^2} e^{-\frac{i}{\hbar}p(x_1-x_{2N+2})}\\ &\quad e^{-\Delta\beta\frac{p^2}{2m}}\end{aligned} \tag{2.6}$$

With this, eq 2.3 becomes

$$\begin{aligned}A_W^\beta(q,p) = {}& \frac{1}{\sqrt{2\pi\hbar}}\sqrt{\frac{\pi m}{2\hbar^2\Delta\beta}}\int dx_1\cdots\int dx_{2N+2}\\ & e^{-\Delta\beta V(x_1)}\langle x_1|e^{-\Delta\beta\hat{T}}|x_2\rangle e^{-\Delta\beta V(x_2)}\langle x_2|e^{-\Delta\beta\hat{T}}|x_3\rangle\\ & \cdots\langle x_N|e^{-\frac{1}{2}\Delta\beta\hat{T}}|x_{N+1}\rangle\langle x_{N+1}|\hat{A}|x_{N+2}\rangle\langle x_{N+2}|e^{-\frac{1}{2}\Delta\beta\hat{T}}|x_{N+3}\rangle\\ & e^{-\Delta\beta V(x_{N+3})}\cdots\langle x_{2N+1}|e^{-\frac{1}{2}\Delta\beta\hat{T}}|x_{2N+2}\rangle e^{-\frac{2m}{\hbar^2\Delta\beta}\left\{q-\left(\frac{x_1+x_{2N+2}}{2}\right)\right\}^2}\\ & e^{-\frac{ip}{\hbar}(x_1-x_{2N+2})}e^{-\Delta\beta\frac{p^2}{2m}}\end{aligned} \tag{2.7}$$

Equation 2.7 contains a Gaussian function of p, which is useful for generating classical trajectory initial conditions. The variable q is now tied to the midpoint of the path integral chain, whose end points can be separated by a large distance at low temperatures. The $\Delta\beta$ coefficient in the Gaussian momentum distribution implies that high momentum values will be sampled, which (given the large values of the end point coordinate difference) gives rise to a rapidly oscillatory phase and a rather severe sign problem. One concludes that neither of the expressions discussed so far are good candidates for Monte Carlo sampling.

b. Coherent State-Based Path Integral Representation of the Wigner Density. On the other hand, it is comparatively easy to calculate the Husimi[25] phase space transform of the operator,

$$A_H(q,p) = \langle g_{q,p}|\hat{A}|g_{q,p}\rangle \tag{2.8}$$

where $|g_{q,p}\rangle$ are coherent states whose wave functions have the standard form

$$\langle q'|g_{q,p}\rangle = \left(\frac{\gamma}{\pi}\right)^{1/4} e^{-\frac{\gamma}{2}(q'-q)^2+\frac{i}{\hbar}p(q'-q)} \tag{2.9}$$

The Wigner and Husimi functions are connected through the relation[28]

$$A_W(q,p) = e^{-\frac{1}{4}\left(\frac{1}{\gamma}\frac{\partial^2}{\partial q^2}+\gamma\frac{\partial^2}{\partial p^2}\right)}A_H(q,p) \tag{2.10}$$

It has been shown[34] that the first order expansion of this expression produces the phase space density derived via the forward−backward semiclassical dynamics (FBSD) approximation of time correlation functions.[35,36]

Our strategy is to obtain the Wigner density by utilizing its relation to the Husimi function, whose numerical evaluation is not as challenging. To proceed, we obtain a discretized path integral representation for the Husimi transform of the symmetrically thermalized operator,

$$A_H^\beta(q,p) = \langle g_{q,p}|e^{-\frac{1}{2}\beta\hat{H}}\hat{A}^\beta e^{-\frac{1}{2}\beta\hat{H}}|g_{q,p}\rangle \tag{2.11}$$

Employing the same factorization of the Boltzmann operator, we obtain

$$\begin{aligned}A_H^\beta(q,p) = {}& \int dx_1\cdots\int dx_{2N+2}\langle g_{q,p}|e^{-\frac{1}{2}\Delta\beta\hat{T}}|x_1\rangle\\ & e^{-\Delta\beta V(x_1)}\langle x_1|e^{-\Delta\beta\hat{T}}|x_2\rangle e^{-\Delta\beta V(x_2)}\langle x_2|e^{-\Delta\beta\hat{T}}|x_3\rangle\\ & \cdots\langle x_N|e^{-\frac{1}{2}\Delta\beta\hat{T}}|x_{N+1}\rangle\langle x_{N+1}|\hat{A}|x_{N+2}\rangle\langle x_{N+2}|e^{-\frac{1}{2}\Delta\beta\hat{T}}|x_{N+3}\rangle\\ & e^{-\Delta\beta V(x_{N+3})}\cdots e^{-\Delta\beta V(x_{2N+2})}\langle x_{2N+2}|e^{-\frac{1}{2}\Delta\beta\hat{T}}|g_{q,p}\rangle\end{aligned} \tag{2.12}$$

Using the analytic expression[37] for the coherent state factors,

$$\begin{aligned}\langle x_k|e^{-\frac{1}{2}\Delta\beta\hat{T}}|g_{q,p}\rangle = {}& \left(\frac{\gamma}{\pi}\right)^{1/4}\sqrt{\frac{2m}{2m+\hbar^2\Delta\beta\gamma}}\\ & e^{-\frac{2m}{2m+\hbar^2\Delta\beta\gamma}\left(\frac{\gamma}{2}(q-x_k)^2+\frac{\Delta\beta}{4m}p^2+ip(q-x_k)\right)}\end{aligned} \tag{2.13}$$

eq 2.12 becomes

DOI: 10.1021/acs.jpca.9b00758
J. Phys. Chem. A 2019, 123, 4284−4294

$$\langle g_{q,p}|\, e^{-\frac{1}{2}\beta\hat{H}}\hat{A}e^{-\frac{1}{2}\beta\hat{H}}|g_{q,p}\rangle = \left(\frac{\gamma}{\pi}\right)^{1/2}\frac{2m}{2m+\hbar^2\Delta\beta\gamma}\int dx_1\cdots\int dx_{2N+2}$$
$$e^{-\Delta\beta V(x_1)}\langle x_1|e^{-\frac{1}{2}\Delta\beta\hat{T}}|x_2\rangle e^{-\Delta\beta V(x_2)}\langle x_2|e^{-\Delta\beta\hat{T}}|x_3\rangle$$
$$\cdots\langle x_N|e^{-\frac{1}{2}\Delta\beta\hat{T}}|x_{N+1}\rangle\langle x_{N+1}|\hat{A}|x_{N+2}\rangle\langle x_{N+2}|e^{-\frac{1}{2}\Delta\beta\hat{T}}|x_{N+3}\rangle$$
$$e^{-\Delta\beta V(x_{N+3})}\cdots e^{-\Delta\beta V(x_{2N+2})}\langle x_{2N+1}|e^{-\frac{1}{2}\Delta\beta\hat{T}}|x_{2N+2}\rangle$$
$$e^{-\frac{2m}{2m+\hbar^2\Delta\beta\gamma}\left(\frac{\gamma}{2}((q-x_1)^2+(q-x_{2N+2})^2)+\frac{\Delta\beta}{2m}p^2+\frac{i}{\hbar}p(x_1-x_{2N+2})\right)} \tag{2.14}$$

The end points of the path integral chain in eq 2.14 are now linked to the coherent state variable q, which closes the necklace. As a result, the distance $|x_1 - x_{2N+2}|$ does not grow exceedingly large, preventing dramatic growth of the phase which would otherwise lead to a sign problem. This is a major computational advantage of coherent state-based expressions compared to their Wigner forms.[26,27] Note also the presence of an exponential factor for the momentum variable, which allows Monte Carlo sampling.

The exponential derivative operator that converts the Husimi function to the Wigner function acts only on the coherent state coordinates. Since eq 2.8 is an ordinary function of q and p, derivatives with respect to q or p commute, and thus may be evaluated in separate steps.

To evaluate the exponential derivatives, we work in Fourier space. Consider an operator of the form $\exp(-\eta\ \partial^2/\partial x^2)$ acting on a Gaussian function $\psi(x) = \exp(-\ ax^2 + bx)$ where $a > 0$. The Fourier transform $\tilde{\psi}(k)$ of $\psi(x)$ is given by

$$\tilde{\psi}(k) = \frac{1}{\sqrt{2\pi}}\int dx\ e^{-ikx}\psi(x) = \frac{1}{\sqrt{2a}}\ e^{\frac{(b-ik)^2}{4a}} \tag{2.15}$$

Using this,

$$e^{-\eta\frac{\partial^2}{\partial x^2}}\psi(x) = \frac{1}{\sqrt{2\pi}}\int dk\ e^{ikx}\ e^{\eta k^2}\ \tilde{\psi}(k)$$
$$= \frac{e^{b^2/4a}}{\sqrt{1-4\eta a}}\exp\left(-\frac{a}{1-4\eta a}\left(x-\frac{b}{2a}\right)^2\right),$$
$$\text{if } 4\eta a < 1 \tag{2.16}$$

Applying eq 2.16, we obtain

$$e^{-\frac{1}{4\gamma}\frac{\partial^2}{\partial q^2}}\ e^{-\frac{m\gamma}{2m+\hbar^2\Delta\beta\gamma}((q-x_1)^2+(q-x_{2N+2})^2)}$$
$$= \sqrt{\frac{2m+\Delta\beta\gamma}{\Delta\beta\gamma}}\ e^{-\frac{2m}{\Delta\beta}\left(q-\frac{x_1+x_{2N+2}}{2}\right)^2}\ e^{-\frac{m\gamma}{2(2m+\Delta\beta\gamma)}(x_1-x_{2N+2})^2} \tag{2.17}$$

$$e^{-\frac{1}{4}\gamma\frac{\partial^2}{\partial p^2}}\ e^{-\frac{2m}{2m+\hbar^2\Delta\beta\gamma}\left(\frac{\Delta\beta}{2m}p^2+ip(x_1-x_{2N+2})\right)}$$
$$= \sqrt{\frac{2m+\Delta\beta\gamma}{2m}}\ e^{-\Delta\beta\frac{p^2}{2m}}\ e^{-\frac{i}{\hbar}p(x_1-x_{2N+2})}\ e^{\frac{m\gamma}{2(2m+\Delta\beta\gamma)}(x_1-x_{2N+2})^2} \tag{2.18}$$

The last Gaussian factor in eq 2.17 has the desirable property of holding the chain end points x_1 and x_{2N+2} close together. However, this factor is exactly canceled by its reciprocal present in eq 2.18, leading to the open chain configuration and rapidly oscillatory phase discussed previously. In fact, upon combining eqs 2.14, 2.17, and 2.18, it is easy to see that all γ-dependent terms cancel and one recovers the expression obtained from direct discretization of the Wigner density, eq 2.7. As discussed earlier, this expression will lead to sampling of open chains with distant end points, and of large momentum values corresponding to a high-temperature distribution.

Rather than allowing phase cancellation to narrow the phase space distribution at the cost of poor Monte Carlo convergence, we propose to replace the integrand with a more confined distribution, which can gradually be broadened until convergence is achieved. The first step involves expanding the inverse Gaussian of eq 2.18 in a truncated polynomial through order n_x,

$$e^{\frac{m\gamma}{2(2m+\Delta\beta\gamma)}(x_1-x_{2N+2})^2} \simeq \sum_{j=0}^{n_x}\frac{1}{j!}\left(\frac{m\gamma(x_1-x_{2N+2})^2}{2(2m+\Delta\beta\gamma)}\right)^j \tag{2.19}$$

Equation 2.19 becomes exact as $n_x \to \infty$. Using this truncation, the Wigner transform becomes

$$A^{\beta}_{W,n_x}(q,p) = \left(\frac{\gamma}{\pi}\right)^{1/2}\sqrt{\frac{2m}{\Delta\beta\gamma}}\int\cdots\int dx_1\cdots dx_{2N+2}e^{-\Delta\beta V(x_1)}\cdots$$
$$\langle x_1|e^{-\Delta\beta\hat{T}}|x_2\rangle e^{-\Delta\beta V(x_2)}\langle x_2|e^{-\Delta\beta\hat{T}}|x_3\rangle\cdots\langle x_N|e^{-\frac{1}{2}\Delta\beta\hat{T}}|x_{N+1}\rangle\cdots$$
$$\langle x_{N+1}|\hat{A}|x_{N+2}\rangle\langle x_{N+2}|e^{-\frac{1}{2}\Delta\beta\hat{T}}|x_{N+3}\rangle e^{-\Delta\beta V(x_3)}\cdots$$
$$\langle x_{2N+1}|e^{-\frac{1}{2}\Delta\beta\hat{T}}|x_{2N+2}\rangle e^{-\Delta\beta V(x_{2N+2})}\cdots$$
$$e^{-\frac{i}{\hbar}p(x_1-x_{2N+2})}e^{-\Delta\beta\frac{p^2}{2m}-\frac{2m}{\Delta\beta}\left(q-\frac{x_1+x_{2N+2}}{2}\right)^2-\frac{m\gamma}{2(2m+\Delta\beta\gamma)}(x_1-x_{2N+2})^2}\cdots$$
$$\sum_{j=0}^{n_x}\frac{1}{j!}\left(\frac{m\gamma(x_1-x_{2N+2})^2}{2(2m+\Delta\beta\gamma)}\right)^j \tag{2.20}$$

Since a Gaussian decays faster than a polynomial of any finite order, the truncated form of eq 2.20 prevents the distance of the chain end points from growing too large.

To narrow the momentum distribution toward the expected Boltzmann form at the given temperature, we insert the Gaussian factor $\exp(-\alpha p^2/2m)$ and its reciprocal, which we subsequently expand through order n_p. This procedure leads us to the following final expression for the Wigner transform of the operator, which contains two truncation parameters, n_x and n_p:

$$A^{\beta}_{W,n_x,n_p}(q,p) = \left(\frac{\gamma}{\pi}\right)^{1/2}\sqrt{\frac{2m}{\Delta\beta\gamma}}\int dx_1\cdots\int dx_{2N+2}$$
$$e^{-\Delta\beta V(x_1)}\langle x_1|e^{-\Delta\beta\hat{T}}|x_2\rangle e^{-\Delta\beta V(x_2)}$$
$$\langle x_2|e^{-\Delta\beta\hat{T}}|x_3\rangle\cdots\langle x_N|e^{-\frac{1}{2}\Delta\beta\hat{T}}|x_{N+1}\rangle$$
$$\langle x_{N+1}|\hat{A}|x_{N+2}\rangle\langle x_{N+2}|e^{-\frac{1}{2}\Delta\beta\hat{T}}|x_{N+3}\rangle$$
$$e^{-\Delta\beta V(x_3)}\cdots e^{-\alpha\frac{p^2}{2m}-\frac{2m}{\Delta\beta}\left(q-\frac{x_1+x_{2N+2}}{2}\right)^2-\frac{m\gamma}{2(2m+\Delta\beta\gamma)}(x_1-x_{2N+2})^2}$$
$$e^{-\frac{i}{\hbar}p(x_1-x_{2N+2})}$$
$$\left(\sum_{j=0}^{n_x}\frac{1}{j!}\left(\frac{m\gamma(x_1-x_{2N+2})^2}{2(2m+\Delta\beta\gamma)}\right)^j\right)\left(\sum_{k=0}^{n_p}\frac{1}{k!}\left((\alpha-\Delta\beta)\frac{p^2}{2m}\right)^k\right) \tag{2.21}$$

We note that the level of truncation required for convergence, that is, the parameters n_x and n_p, can be different for different degrees of freedom, and that the rate of convergence also depends on the observable under consideration.

Equation 2.21 is the final expression of the CSPIW method. The coherent state factor γ is estimated from the width of the ground state wave function or the quantum dispersion of the particles. An accurate estimation of the coherent state parameter is not necessary for convergence. The Gaussian parameter α is to be chosen based on physical intuition. Good choices of α lead to convergence with smaller values of n_p. At relatively high temperatures, one expects the classical Boltzmann distribution to provide a reasonable approximation to the momentum dependence of the Wigner distribution, so

DOI: 10.1021/acs.jpca.9b00758
J. Phys. Chem. A 2019, 123, 4284−4294

a sensible choice is in this case $\alpha = \beta$, the inverse temperature. Another choice results from the momentum dependence of the harmonic approximation, which suggests the value

$$\alpha = \frac{2}{\omega\hbar}\tanh\left(\frac{1}{2}\hbar\omega\beta\right) \tag{2.22}$$

where ω is the frequency of the harmonic fit to the potential. It is important to note that the correctness of the resulting Wigner distribution is not dependent upon the choice of α, which only affects the rate of convergence with respect to the truncation parameters.

The entire integrand of eq 2.21, apart from the phase, can be used as the Monte Carlo sampling function. In the rest of this paper, we focus on the Wigner function corresponding to the thermal density operator, obtained by setting $\hat{A} = 1$, which introduces the delta function $\delta(x_{N+2} - x_{N+1})$ in the integrand. Since the Wigner function is real-valued, the imaginary part of the integrand must integrate to zero. The CSPIW expression for the thermal Wigner density, which we label $W^{\beta}_{n_x, n_p}(q, p)$, is thus given by the expression

$$W^{\beta}_{n_x,n_p}(q, p) = \int \mathrm{d}x_1 \cdots \int \mathrm{d}x_{2N+2}\, f(q, p, x_1, x_2, \cdots x_{2N+2}) g(x_1, x_{2N+2}) \tag{2.23}$$

with

$$\begin{aligned} f(q, p, x_1, x_2, \cdots x_{2N+2}) = {} & \left(\frac{\gamma}{\pi}\right)^{1/2} \sqrt{\frac{2m}{\Delta\beta\gamma}}\, \mathrm{e}^{-\Delta\beta V(x_1)} \langle x_1|\mathrm{e}^{-\Delta\beta\hat{T}}|x_2\rangle \\ & \mathrm{e}^{-\Delta\beta V(x_2)} \langle x_2|\mathrm{e}^{-\Delta\beta\hat{T}}|x_3\rangle \cdots \langle x_N|\mathrm{e}^{-\frac{1}{2}\Delta\beta\hat{T}}|x_{N+1}\rangle \delta(x_{N+2} - x_{N+1}) \langle x_{N+2}| \\ & \mathrm{e}^{-\frac{1}{2}\Delta\beta\hat{T}}|x_{N+3}\rangle \mathrm{e}^{-\Delta\beta V(x_3)} \\ & \cdots \mathrm{e}^{-\alpha\frac{p^2}{2m} - \frac{2m}{\Delta\beta}\left(q - \frac{x_1 + x_{2N+2}}{2}\right)^2 - \frac{m\gamma}{2(2m+\Delta\beta\gamma)}(x_1 - x_{2N+2})^2} \\ & \left(\sum_{j=0}^{n_x} \frac{1}{j!}\left(\frac{m\gamma(x_1 - x_{2N+2})^2}{2(2m + \Delta\beta\gamma)}\right)^j\right)\left(\sum_{k=0}^{n_p} \frac{1}{k!}\left((\alpha - \Delta\beta)\frac{p^2}{2m}\right)^k\right) \end{aligned} \tag{2.24}$$

and

$$g(x_1, x_{2N+2}) = \cos(p(x_1 - x_{2N+2})/\hbar) \tag{2.25}$$

We emphasize again that once convergence with respect to n_x and n_p is achieved, eqs 2.23 and 2.24 produce the exact Wigner density $W(q, p)$.

By virtue of the delta function in eq 2.24, the CSPIW expression for the Wigner density has $2N + 1$ integration variables for each degree of freedom. Evaluation of this high-dimensional integral requires the use of Monte Carlo methods,[38] and the non-negative function f is the natural choice of sampling function. Since the Wigner function is normalized, the product fg integrates to unity, therefore the sampling function is not normalized. To evaluate the Wigner function itself, one would need to compute the normalization integral of the sampling function by other methods. However, this is not necessary in the most common use of the Wigner density, in the context of quasiclassical approximations.

Quasiclassical dynamics calculations require trajectory initial conditions with weights given by the Wigner density. In multidimensional applications, the initial conditions must be sampled via Monte Carlo methods, thus the integrals with respect to the auxiliary path integral variables must be evaluated concurrently with those required to construct the Wigner function. As an example, consider the real part of the quasiclassical position correlation function, which is given by the expression

$$\begin{aligned} C(t) &= \int \mathrm{d}q_0 \int \mathrm{d}p_0 W(q_0, p_0) q_0 q(t) \\ &= \int \mathrm{d}q_0 \int \mathrm{d}p_0 \int \mathrm{d}x_1 \cdots \int \mathrm{d}x_{2N+1} \int \mathrm{d}x_{2N+2} \\ &\quad f(q_0, p_0, x_1, x_2, \cdots x_{2N+2}) g(x_1, x_{2N+2}) q_0 q(t) \end{aligned} \tag{2.26}$$

with $2N + 3$ integration variables, which is in a form suitable for Monte Carlo evaluation with $f \geq 0$ as the unnormalized sampling function. If desired, the imaginary part can be obtained from the real part by using the relation between the real and imaginary parts of an autocorrelation function.[22,39,40] We rewrite this expression as the ratio

$$C(t) = \frac{\int \mathrm{d}q_0 \int \mathrm{d}p_0 W(q_0, p_0) q_0 q(t)}{\int \mathrm{d}q_0 \int \mathrm{d}p_0 W(q_0, p_0)} = \frac{\int \mathrm{d}q_0 \int \mathrm{d}p_0 \int \mathrm{d}x_1 \cdots \int \mathrm{d}x_{2N+1} \int \mathrm{d}x_{2N+2} f(q_0, p_0, x_1, x_2, \cdots x_{2N+2}) g(x_1, x_{2N+2}) q_0 q(t)}{\int \mathrm{d}q_0 \int \mathrm{d}p_0 \int \mathrm{d}x_1 \cdots \int \mathrm{d}x_{2N+1} \int \mathrm{d}x_{2N+2} f(q_0, p_0, x_1, x_2, \cdots x_{2N+2}) g(x_1, x_{2N+2})} \tag{2.27}$$

By computing the integral of the denominator of eq 2.27, along with that of the numerator, using the same sampling function, the normalization factors cancel upon division, thus numerical evaluation of the normalization integral is not necessary.

c. CSPIW Sampling with Information-Guided Noise Reduction. The CSPIW formulation achieves a significant reduction of the phase fluctuations, leading to a dramatic reduction of the Monte Carlo error. Still, application of the method to systems of many degrees of freedom at low temperature, where many path integral beads are necessary, can be challenging. To further reduce the statistical error, we resort to IGNoR,[29] a technique that exploits the exact value of a similar integral. IGNoR has been used successfully in FBSD simulations of neat fluids at low temperatures.[41,42] In this section we describe the use of IGNoR to reduce the Monte Carlo noise in the evaluation of the CSPIW expression.

To proceed, we note that the converged CSPIW Wigner function is normalized to unity; that is,

$$\int \mathrm{d}q_0 \int \mathrm{d}p_0 W(q_0, p_0) = \int \mathrm{d}q_0 \int \mathrm{d}p_0 \int \mathrm{d}x_1 \cdots \int \mathrm{d}x_{2N+2}\, f(q_0, p_0, x_1, x_2, \cdots x_{2N+2}) g(x_1, x_{2N+2}) = 1 \tag{2.28}$$

We define the integrals of the positive and negative regions of the Wigner integrand,

$$I_{\pm} = \int \mathrm{d}q_0 \int \mathrm{d}p_0 \int \mathrm{d}x_1 \cdots \int \mathrm{d}x_{2N+2} f(q_0, p_0, x_1, x_2, \cdots x_{2N+2}) g(x_1, x_{2N+2}) \Theta(\pm g) \tag{2.29}$$

and the change of the values of these integrals upon multiplication with the desired position correlation factors,

DOI: 10.1021/acs.jpca.9b00758
J. Phys. Chem. A 2019, 123, 4284−4294

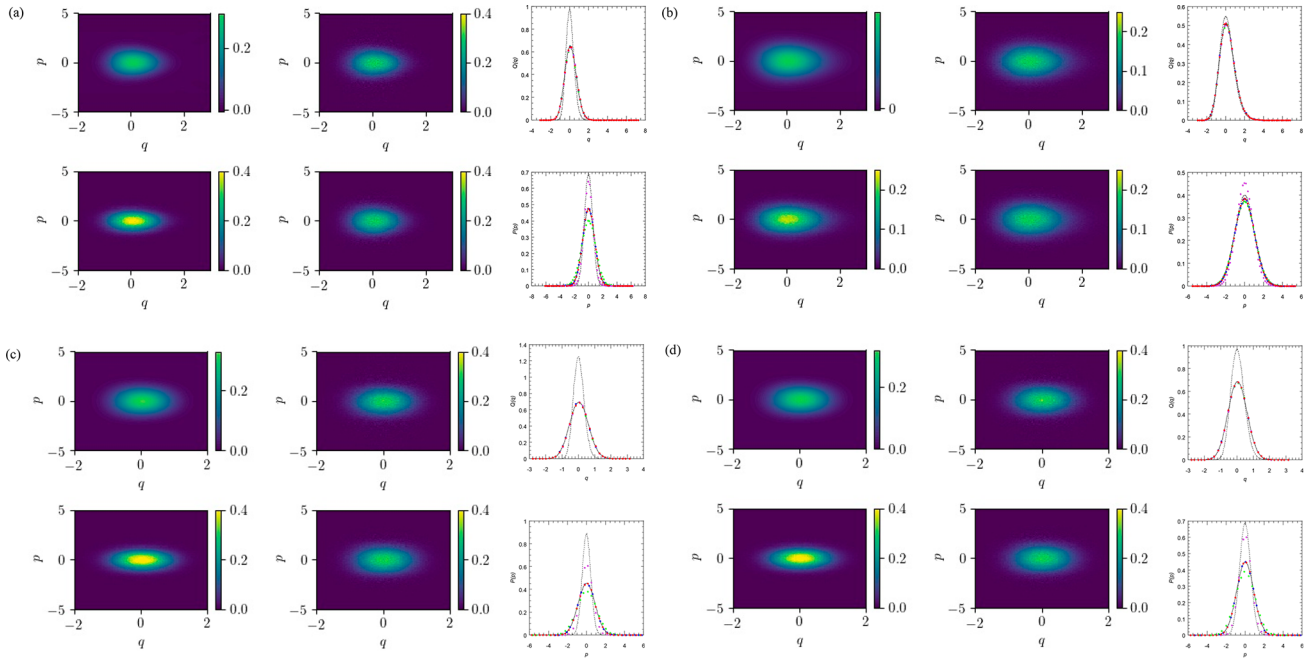

Figure 1. Contour maps: two-dimensional histograms of the phase space density. Converged basis set calculations (top left), $W_{3,\infty}(q, p)$ (top right), $W_{3,0}(q, p)$ (bottom left), $W_{3,4}(q, p)$ (bottom right). The line plots present the marginal distributions, obtained by integrating the Wigner function with respect to p and q, respectively. Solid black line, basis set calculations; dashed black line, classical Boltzmann density; green markers, $W_{0,\infty}(q, p)$; purple markers, $W_{3,0}(q, p)$; blue markers, $W_{3,\infty}(q, p)$; red markers, $W_{3,4}(q, p)$. (a) Model potential V_1, $\hbar\omega\beta = 3\sqrt{2}$, $N = 7$. (b) Model potential V_1, $\hbar\omega\beta = \sqrt{2}$, $N = 2$. (c) Model potential V_2, $\hbar\omega\beta = 5\sqrt{2}$, $N = 12$. (d) Model potential V_2, $\hbar\omega\beta = 3\sqrt{2}$, $N = 7$.

$$C_{\pm}(t) = \int dq_0 \int dp_0 \int dx_1 \cdots \int dx_{2N+2} f(q_0, p_0, x_1, x_2, \cdots x_{2N+2}) g(x_1, x_{2N+2}) q_0 q(t) \Theta(\pm g) \tag{2.30}$$

The exact value of the correlation function is given by $C_+ + C_-$, and this value often is very small compared to the magnitudes of C_+ and C_-. The integrals in eqs 2.29 and 2.30 correspond to the volumes of the positive and negative regions of these functions, and are easily evaluated with relatively good statistics. However, the cancellation between positive and negative volumes gives rise to very poor statistics, commonly referred to as a Monte Carlo sign problem. The IGNoR technique exploits the fact that the Monte Carlo estimates (from the same random walk) of the integrals of eq 2.30 are strongly correlated with those of eq 2.29. However, the exact values of the integrals in eq 2.29 are available. Thus, IGNoR replaces the noisy term $\langle C_- \rangle$ in the raw Monte Carlo estimate $\langle C_+ \rangle + \langle C_- \rangle$ by a corrected estimate,

$$\langle C(t) \rangle = \langle C_+(t) \rangle + \langle C_-(t) \rangle \frac{1 - \langle I_+ \rangle}{\langle I_- \rangle} \tag{2.31}$$

where the angular brackets indicate the raw Monte Carlo averages. It has been shown[29,41,42] that the IGNoR correction leads to substantial noise cancellation, which often results in a dramatic reduction of statistical error.

III. APPLICATIONS

In this section we investigate the convergence characteristics of the procedure described in section II by applying it to several one-dimensional model Hamiltonians and also to systems of many degrees of freedom. We show two-dimensional plots of the phase space density, the resulting position-and momentum-space densities, as well as the quasiclassical approximation to time correlation functions obtained from trajectories sampled from the Wigner distribution. All time correlation functions are obtained through classical trajectory calculations using the velocity Verlet algorithm to solve Newton's equations. The error bars correspond to the standard deviation of the mean calculated by binning the Monte Carlo data.

Further, we compare the CSPIW results to those obtained analytically or via numerically exact basis set methods, and to the results of three approximate procedures: the local harmonic and Gaussian approximations, and the adiabatic switching trajectory-based method. Before presenting our results we give a short overview of these methods.

The local harmonic approximation (LHA) and local Gaussian approximation (LGA) can both be expressed as

$$W_{\mathrm{LGA\,or\,LHA}}(q, p) = \langle q | e^{-\beta H} | q \rangle \left(\frac{\beta}{2\pi m Q(u)} \right)^{1/2} \exp\left(-\beta \frac{p^2}{2m} \frac{1}{Q(u)} \right) \tag{3.1}$$

where $u(q) = \hbar\beta\omega(q)$ (with $\omega(q) = \sqrt{V''(q)/m}$) and

$$Q(u) = \frac{\frac{1}{2}u}{\tanh\left(\frac{1}{2}u\right)} \tag{3.2}$$

Equation 3.1 is applicable to regions of positive curvature, where $\omega(q)$ is real-valued. At points where $\omega(q)$ is imaginary the LHA replaces eq 3.2 by

$$Q(u) = \frac{\frac{1}{2}|u|}{\tan\left(\frac{1}{2}|u|\right)}, \quad |u| < \pi \tag{3.3}$$

DOI: 10.1021/acs.jpca.9b00758
J. Phys. Chem. A 2019, 123, 4284−4294

When $|u| > \pi$, Q becomes negative and the LHA is not usable. The LGA suggests using

$$Q(u) = \frac{\tanh\left(\frac{1}{2}|u|\right)}{\frac{1}{2}|u|} \tag{3.4}$$

in regions of negative curvature.

The adiabatic switching method for generating the Wigner density[21,22] (ASW) relies on the classical adiabatic theorem to slowly convert the available Wigner density of a model reference system (e.g., a quadratic fit to the potential) to that of the target Hamiltonian. Because the adiabatic switching process changes the energy of the trajectories, a rescaling procedure is also employed to maintain the desired temperature. The ASW approximation becomes exact for quadratic potentials.

A. One-Dimensional Models. We demonstrate the method on three strongly anharmonic one-dimensional models with particle mass $m = 1$.

The first two models employ the potentials V_1 and V_2, which are given by fourth degree polynomials,

$$V_1(q) = \frac{1}{2}\omega^2 q^2 - 0.2q^3 + 0.015q^4 \tag{3.5}$$

$$V_2(q) = \frac{1}{2}\omega^2 q^2 - 0.1q^3 + 0.1q^4 \tag{3.6}$$

where $\omega = \sqrt{2}$. Figure 1 shows the phase space distribution at two temperatures for each of the potentials. We also compare the position and momentum distributions

$$P(p) = \int dq W(q, p),\ Q(q) = \int dp W(q, p) \tag{3.7}$$

obtained via the CSPIW method to those obtained via numerically exact basis set calculations and also to the classical Boltzmann distribution. The CSPIW calculations employed 10^6 Monte Carlo samples. The reason for using such a large number of Monte Carlo points was our desire to generate smooth, visually appealing phase space distributions. Thermodynamic averages and time-dependent properties extracted from quasiclassical calculations with initial conditions sampled from the CSPIW distribution require much smaller numbers of Monte Carlo points. Because convergence of the $2N + 3$-dimensional integral was relatively easy in this case, we did not apply the IGNoR enhancement.

It is seen that the CSPIW calculation converges to the correct phase space distribution over a wide range of temperatures for both potentials, accurately capturing the position and momentum spans as well as the position of the peak which is slightly shifted from the potential minimum. Further, Figure 1 shows that the position distribution is always in excellent agreement with the basis set results, regardless of the values of the truncation parameters. At low temperatures, the number of beads required to minimize the Trotter error increases and the span of the path integral chain grows, leading to a larger and more oscillatory phase. The CSPIW expansion shrinks the highly oscillatory wings responsible for this phase substantially, such that the distribution converges well even at very low temperatures. Convergence was achieved with $n_x = 3$, $n_p = 4$.

Next, we examine the use of the CSPIW distribution to obtain time-dependent properties from a classical trajectory calculation. Figure 2 shows the real part of the position correlation function, eq 2.26, obtained by launching classical trajectories from the CSPIW distribution $W_{3,4}$, the LHA approximation, and also from the exact Wigner function, obtained through a basis set calculation. The calculations were performed at very low temperatures, which are most challenging for the CSPIW method. It is seen that the converged CSPIW density leads to results practically indistinguishable from those obtained by using the exact Wigner function.

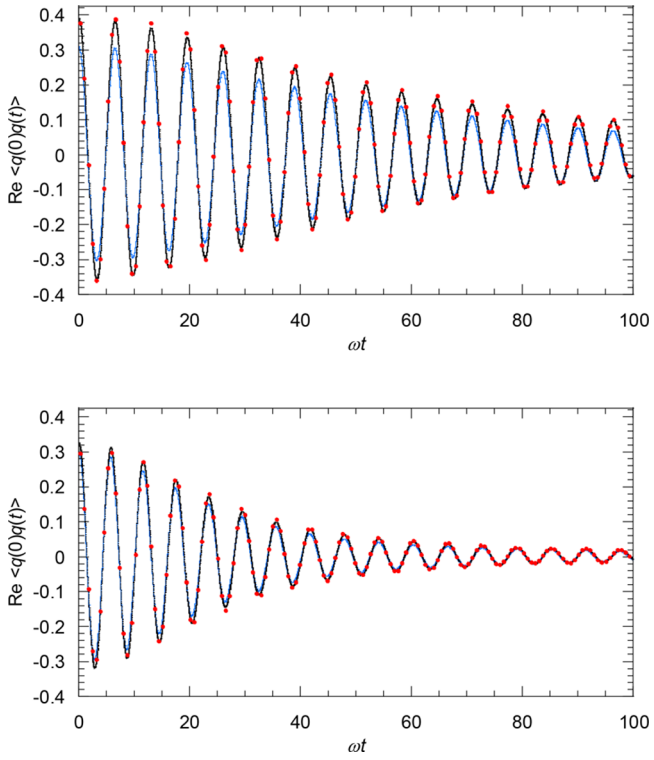

Figure 2. Real part of the quasiclassical position autocorrelation function. Black line: Wigner dynamics starting from the exact Wigner function with 10^5 Monte Carlo points. Blue line: Wigner dynamics starting from the LHA Wigner density. Red circles: CSPIW results with $W_{3,4}$. Top: model potential V_1, $\hbar\omega\beta = 3\sqrt{2}$, $N = 7$. Bottom: model potential V_2, $\hbar\omega\beta = 5\sqrt{2}$, $N = 12$.

The third model system is a Morse potential,

$$V(x) = D(1 - e^{-\alpha(q-q_0)})^2 \tag{3.8}$$

with $D = \frac{11}{4}$, $\alpha = \sqrt{\frac{2}{11}}$, which lead to the harmonic frequency at the minimum $\omega_{min} = 1$. With these parameters, the potential supports six bound states.

In Figure 3 we present the Wigner phase space distribution at $\hbar\omega_{min}\beta = 10$ as obtained using the $W_{4,4}$ CSPIW procedure, and also from the LGA and ASW approximations. The chosen low temperature leads to extended imaginary time paths which cause substantial phase cancellation and thus present a challenge to the CSPIW calculation. Excited state contributions are negligible at this temperature, so we also present a comparison to the analytical expression for the ground state, which is seen to have very small negative zones in the wings. It is seen that the CSPIW method faithfully reproduces the shape of the Wigner density with good statistics, although the very small negative parts are obscured by Monte Carlo noise. This potential has an extended region of negative curvature, where $|u| > \pi$. As a result, the LHA approximation breaks

DOI: 10.1021/acs.jpca.9b00758
J. Phys. Chem. A 2019, 123, 4284−4294

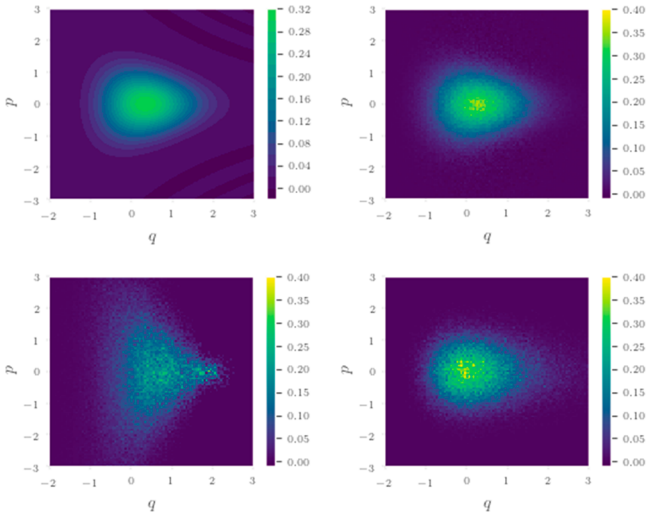

Figure 3. Wigner density for the Morse potential at $\hbar\omega_{min}\beta = 10$. Top left: Analytic ground state Wigner function. Top right: $W_{4,4}$. Bottom left: LGA aproximation. Bottom right: ASW approximation.

down completely, and we do not show it in the figure. The LGA density displays a sharp cutoff with a high ridge in the repulsive potential region when $u > \pi$ and a much more extended momentum distribution along the ridge. The simple, trajectory-based ASW approximation does a very good job of capturing the phase space density.

B. System-Bath Model. Next, we use the CSPIW method to generate the Wigner function and subsequent dynamics for a harmonic system coupled bilinearly to a dissipative harmonic bath. This model provides an excellent testbed for assessing the convergence properties of the CSPIW method, as the discretized path integral representation and integrand truncation do not benefit from the quadratic nature of the Hamiltonian, yet obtaining exact results is relatively straightforward. The system-bath Hamiltonian has the form

$$\hat{H} = \frac{\hat{p}_s^2}{2m} + \frac{1}{2}m\Omega^2\hat{s}^2 + \sum_{j=1}^{M}\frac{\hat{p}_j^2}{2m} + \frac{1}{2}m\omega_j^2\hat{x}_j^2 - \sum_j c_j\hat{s}\hat{x}_j \tag{3.9}$$

The frequencies for the harmonic bath and the system-bath coupling coefficients are collectively characterized by a spectral density[43] of the Ohmic form with an exponential cutoff,

$$J(\omega) = \frac{\pi}{2}\hbar\xi\omega e^{-\omega/\omega_c} \tag{3.10}$$

where ξ quantifies the system-bath interaction strength and $\omega_c = 1.25\Omega$. Results are reported for a weakly coupled harmonic bath ($\xi = 0.2$) at a low temperature ($\hbar\Omega\beta = 5$), as well as a strongly coupled bath ($\xi = 1$) at an intermediate temperature ($\hbar\Omega\beta = 2$). In each case the continuous bath was discretized into 24 oscillators using the logarithmic discretization[44,45] with $\omega_{max} = 4\omega_c$. We report the real part of the position autocorrelation function for the system given by the quasiclassical Wigner procedure,

$$\mathrm{ReC}(t) = \int ds_0 \int dp_{s,0} \int d\mathbf{x}_0 \int d\mathbf{p}_0 W(s_0, p_{s,0}, \mathbf{x}_0, \mathbf{p}_0) s_0 s(t) \tag{3.11}$$

Since the Hamiltonian is quadratic, the quasiclassical expression is expected to produce the exact quantum mechanical result, provided the Wigner distribution is accurate.

The CSPIW calculations were performed with $N_s = 16$ for the system coordinate and different numbers of path integral steps for each bath degree of freedom, chosen to give $\hbar\omega_i\beta/N_i \leq 0.4$ This discretization resulted in 372 coordinate plus 25 momentum integration variables in eq 3.11 in the case of the low-temperature bath, and 166 coordinate plus 25 momentum integration variables in the case of the intermediate-temperature bath. Because of the high dimensionality of the integration, we applied the IGNoR convergence enhancement.

Figure 4 shows the quasiclassical results obtained using the CSPIW distribution, along with exact quantum mechanical results calculated analytically, and classical results obtained by sampling trajectory initial conditions from the classical Boltzmann density. For these multidimensional calculations, the integrand truncation implemented in the CSPIW method is essential for convergence, as the sign problem grows exponentially with integral dimension. In the absence of truncation, we found it impossible to obtain meaningful results that were not buried in statistical noise. The correlation functions shown in Figure 3 were evaluated by sampling the $W_{2,0}$ distribution with 25000 Monte Carlo points per dimension. While the CSPIW procedure leads to results with reasonable precision (the statistical error bars are smaller than the marker size), the Monte Carlo error bars in the raw CSPIW results are still substantial. As seen in Figure 3, the IGNoR processing leads to a very significant reduction of

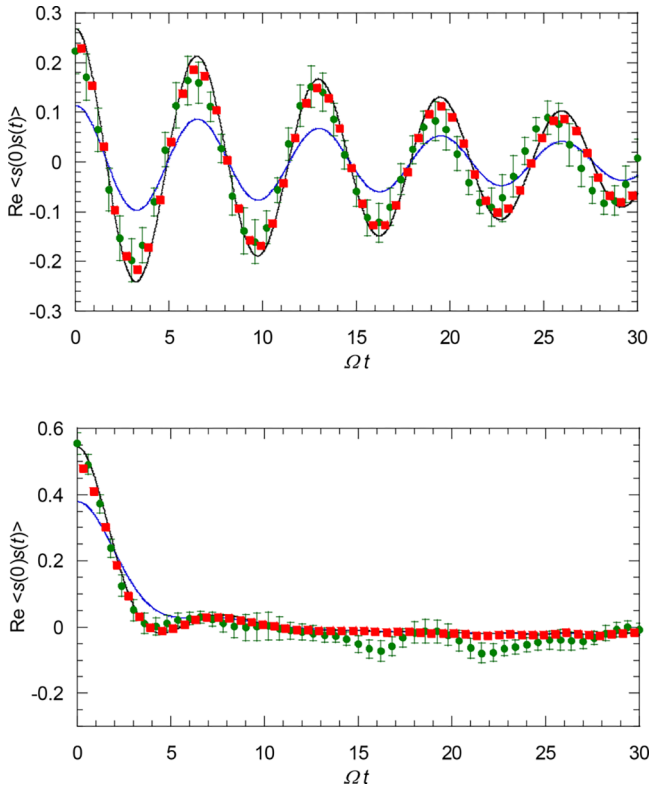

Figure 4. System position autocorrelation function for the system-bath Hamiltonian. Black line: exact quantum mechanical results. Blue line: classical Boltzmann result. Green circles: raw CSPIW results. Red squares: CSPIW method with IGNoR processing. Top: $\omega_c = 1.25\ \Omega$, $\xi = 0.2$, $\hbar\Omega\beta = 5$, 397 integration variables. Bottom: $\omega_c = 1.25\Omega$, $\xi = 1$, $\hbar\Omega\beta = 2$, 191 integration variables.

DOI: 10.1021/acs.jpca.9b00758
J. Phys. Chem. A 2019, 123, 4284−4294

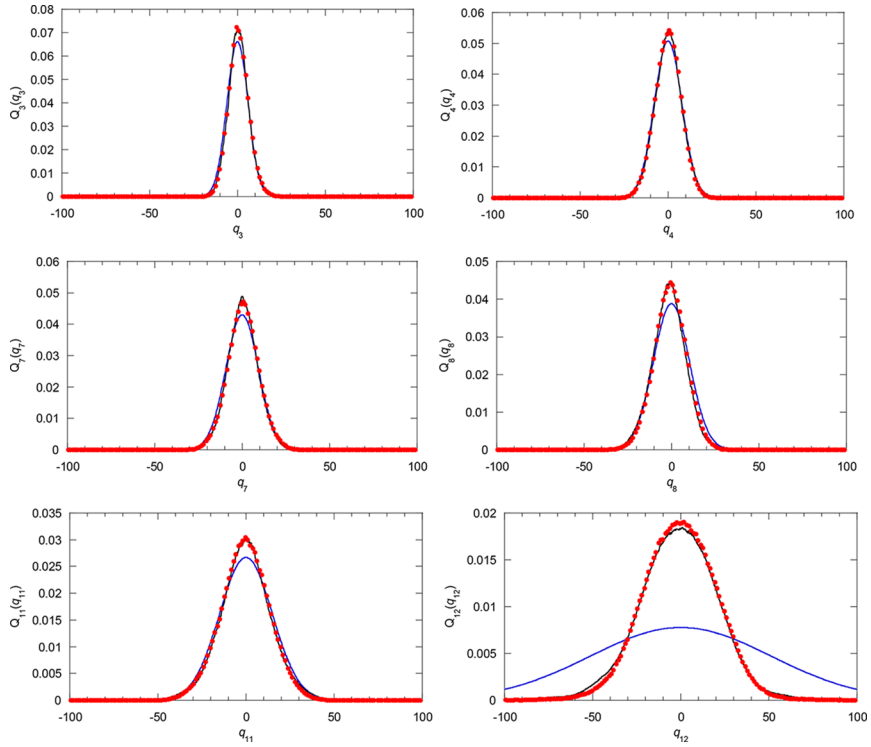

Figure 5. Marginal position distributions of some normal modes of formamide at 300 K. Black solid line: exact quantum PIMC results. Blue dashed line: harmonic Wigner distribution. Red markers: $W_{2,0}$ results.

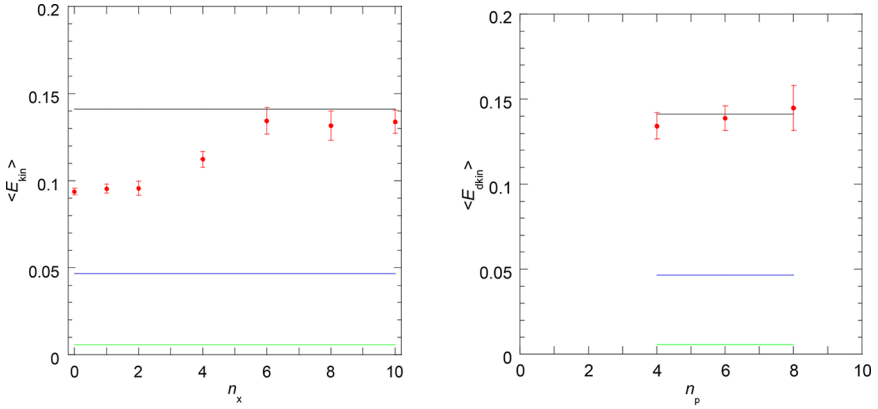

Figure 6. Average vibrational kinetic energy of formamide. Red markers: CSPIW results (with error bars). Green line: classical approximation. Blue line: harmonic Wigner approximation. Black line: PIMC value. Left: convergence of kinetic energy with respect to n_x for n_p = 4. Right: convergence with respect to n_p for n_x = 4.

statistical error, resulting in CSPIW results that are in nearly quantitative agreement with those of the exact calculation. Since the Hamiltonian in eq 3.9 is fully quadratic, the LHA for the Wigner distribution would produce the exact results for this system.

C. Quartic Force Field for Formamide. As a final example, we apply the CSPIW method to the formamide molecule, $HCONH_2$, described by an *ab initio* quartic force field. The potential was calculated using Gaussian 09[46] at the level of Møller−Plesset (MP2) perturbation theory with aug-ccpvtz basis set.[47,48] The Hamiltonian is expressed in normal mode coordinates and has the form

$$\hat{H} = \sum_{j=1}^{n} \frac{1}{2}\hat{p}_j^2 + V(\hat{\mathbf{q}}) \tag{3.12}$$

where n = 12 and

$$V(\mathbf{q}) = \sum_{i=1}^{n} \frac{1}{2}f_{ii}q_i^2 + \frac{1}{6}f_{iii}q_i^3 + \frac{1}{24}f_{iiii}q_i^4 + \sum_{i\neq j\neq \mathrm{k}}^{n} f_{ijk}q_iq_jq_k + \sum_{i\neq j}^{n} \frac{1}{2}f_{iik}q_i^2q_j + \sum_{i\neq j\neq k\neq l}^{n} f_{ijkl}q_iq_jq_kq_l + \sum_{i\neq j}^{n}\left(\frac{1}{6}f_{iiij}q_i^3q_j + \frac{1}{4}f_{iijj}q_i^2q_j^2\right) + \sum_{i\neq j\neq k}^{n} \frac{1}{2}f_{iijk}q_i^2q_jq_k \tag{3.13}$$

We report the marginal thermal distributions of various modes,

DOI: 10.1021/acs.jpca.9b00758
J. Phys. Chem. A 2019, 123, 4284−4294

$$Q_i(q_i) = \int_{-\infty}^{\infty} dq_1 \cdots \int_{-\infty}^{\infty} dq_{i-1} \int_{-\infty}^{\infty} dq_{i+1} \int_{-\infty}^{\infty} dq_n \int_{-\infty}^{\infty} dp_1 \cdots \int_{-\infty}^{\infty} dp_n W(q_1, \cdots, q_n, p_1, \cdots, p_n) \quad (3.14)$$

as obtained using the CSPIW method, along with numerically exact results obtained from path integral Monte Carlo (PIMC) calculations and Wigner distributions corresponding to the harmonic part of the Hamiltonian at 300 K. At this temperature $\hbar\omega_{min}\beta = 0.64$ and $\hbar\omega_{max}\beta = 18.06$, where ω_{min} and ω_{max} are the lowest and highest frequency normal modes, respectively. Each normal mode coordinate was discretized with a different value of time steps, with $2N$ ranging between 4 and 64, with the total number of integration variables equal to 432. For sampling the phase space, 23 000 Monte Carlo points per integration variable were used.

Figure 5 shows the marginal distributions of various normal modes as obtained from the CSPIW method with integrand truncation at $n_x = 2$, $n_p = 0$ and compares them to those obtained from numerically exact PIMC calculations and also to the harmonic approximation. It is seen that the CSPIW results are in excellent agreement with the exact quantum mechanical distributions. While the harmonic approximation appears nearly quantitative for the highest frequency modes, it leads to large error in the distributions of low frequency modes, where the anharmonicity is most pronounced.

We also present the average kinetic energy of the formamide molecule at 300 K. In this calculation we did not apply momentum truncation to the four highest frequency modes, as convergence was easily attained without truncation of these variables. Figure 6 shows the obtained kinetic energy as a function of the truncation parameters. Convergence was achieved with $n_x = 6$, $n_p = 4$. For comparison, we also show the classical kinetic energy, the value obtained from the harmonic approximation to the Wigner function, and also that obtained from numerically exact PIMC calculations. The kinetic energy is obtained as the difference between total and potential energy using the thermodynamic PIMC estimator,[49]

$$\langle E_{kin} \rangle = \langle E \rangle - \langle V \rangle = -\frac{1}{Z}\frac{\partial Z}{\partial \beta} - \langle V \rangle = \left\langle \frac{n}{2\Delta\beta} - \frac{m}{2\hbar^2 N \Delta\beta^2} \sum_{k=1}^{N} |\mathbf{x}_k - \mathbf{x}_{k+1}|^2 \right\rangle \quad (3.15)$$

where $Z = \mathrm{Tr}[\exp(-\beta\hat{H})]$ is the partition function and the brackets denote the normalized Monte Carlo average with respect to the path integral discretization of the Boltzmann operator.

As seen in Figure 6, the converged CSPIW results are in quantitative agreement with the PIMC values. The classical estimate is very poor, as most vibrations are cold at room temperature. The large deviation from the harmonic kinetic energy arises mainly from the large anharmonicity of the lowest frequency mode. Since the number of Monte Carlo samples was kept constant across all the simulations, the statistical error is more pronounced in the CSPIW calculations with higher order truncation parameters.

IV. CONCLUDING REMARKS

We have described in this paper a numerically exact procedure for computing thermal Wigner phase space distributions in systems of many degrees of freedom. The method is based on the path integral representation of the Boltzmann operator, but makes use of the coherent state distribution which involves a stable procedure to minimize the Monte Carlo sign problem by avoiding highly oscillatory regions that do not make an appreciable contribution to the result. We also show how the method may be combined with the IGNoR enhancement to further shrink the statistical error.

Our test calculations on several model systems, including one-dimensional and multidimensional Hamiltonians, show that the CSPIW method quickly leads to converged, numerically exact results with small statistical error for the quantum phase space distribution and also for time correlation functions obtained via classical trajectories. Thus, the CSPIW method should offer a useful tool for quantizing trajectory initial conditions in quasiclassical simulations and also in quantum-classical calculations.

AUTHOR INFORMATION

Corresponding Author

*E-mail: nmakri@illinois.edu.

ORCID

Amartya Bose: 0000-0003-0685-5096

Nancy Makri: 0000-0002-3310-7328

Notes

The authors declare no competing financial interest.

ACKNOWLEDGMENTS

This material is based upon work supported by the National Science Foundation under Award CHE-1665281.

REFERENCES

(1) Wigner, E. J. Calculation of the Rate of Elementary Association Reactions. *J. Chem. Phys.* **1937**, *5*, 720.

(2) Heller, E. J.; Brown, R. C. Errors in the Wigner approach to quantum dynamics. *J. Chem. Phys.* **1981**, *75*, 1048−1050.

(3) Wang, H.; Sun, X.; Miller, W. H. Semiclassical approximations for the calculation of thermal rate constants for chemical reactions in complex molecular systems. *J. Chem. Phys.* **1998**, *108*, 9726−9736.

(4) Sun, X.; Wang, H.; Miller, W. H. Semiclassical theory of electronically nonadiabatic dynamics: Results of a linearized approximation to the initial value representation. *J. Chem. Phys.* **1998**, *109*, 7064−7074.

(5) Miller, W. H. Generalization of the linearized approximation to the semiclassical initial value representation for reactive flux correlation functions. *J. Phys. Chem. A* **1999**, *103*, 9384−9387.

(6) Poulsen, J. A.; Nyman, G.; Rossky, P. J. Practical evaluation of condensed phase quantum correlation functions: A Feynman–Kleinert variational linearized path integral method. *J. Chem. Phys.* **2003**, *119*, 12179−12193.

(7) Liu, J. Path integral Liouville dynamics for thermal equilibrium systems. *J. Chem. Phys.* **2014**, *140*, 140.

(8) Liu, J.; Zhang, Z. Path integral Liouville dynamics: Applications to infrared spectra of OH, water, ammonia, and methane. *J. Chem. Phys.* **2016**, *144*, No. 034307.

(9) Meyer, H.-D.; Miller, W. H. A classical analog for electronic degrees of freedom in nonadiabatic collision processes. *J. Chem. Phys.* **1979**, *70*, 3214−3223.

(10) Stock, G.; Thoss, M. Semiclassical description of nonadiabatic quantum dynamics. *Phys. Rev. Lett.* **1997**, *78*, 578−581.

(11) Miller, W. H.; Cotton, S. J. Classical molecular dynamics simulation of electronically non-adiabatic processes. *Faraday Discuss.* **2016**, *195*, 9.

(12) Hsieh, C. Y.; Kapral, R. Nonadiabatic dynamics in open quantum-classical systems: Forward-backward trajectory solution. *J. Chem. Phys.* **2012**, *137*, 22A507.

DOI: 10.1021/acs.jpca.9b00758
J. Phys. Chem. A 2019, 123, 4284−4294

(13) Kapral, R. Quantum dynamics in open quantum-classical systems. *J. Phys.: Condens. Matter* **2015**, *27*, No. 073201.
(14) Lambert, R.; Makri, N. Quantum-classical path integral: Classical memory and weak quantum nonlocality. *J. Chem. Phys.* **2012**, *137*, 22A552.
(15) Lambert, R.; Makri, N. Quantum-classical path integral: Numerical formulation. *J. Chem. Phys.* **2012**, *137*, 22A553.
(16) Makri, N. Quantum-classical path integral: A rigorous approach to condensed phase dynamics. *Int. J. Quantum Chem.* **2015**, *115*, 1209−1214.
(17) Shi, Q.; Geva, E. Semiclassical theory of vibrational energy relaxation in the condensed phase. *J. Phys. Chem. A* **2003**, *107*, 9059−9069.
(18) Liu, J.; Miller, W. H. Using the thermal Gaussian approximation for the Boltzmann operator in semiclassical initial value time correlation functions. *J. Chem. Phys.* **2006**, *125*, 224104.
(19) Heller, E. J. Time-dependent variational approach to semiclassical dynamics. *J. Chem. Phys.* **1976**, *64*, 63−73.
(20) Shao, J.; Pollak, E. A new time evolving Gaussian series representation of the imaginary time propagator. *J. Chem. Phys.* **2006**, *125*, 133502.
(21) Bose, A.; Makri, N. Evaluation of the Wigner distribution via classical adiabatic switching. *J. Chem. Phys.* **2015**, *143*, 114114.
(22) Bose, A.; Makri, N. Wigner Distribution by Adiabatic Switching in Normal Mode or Cartesian Coordinates and Molecular Applications. *J. Chem. Theory Comput.* **2018**, *14*, 5446−5458.
(23) Montoya-Castillo, A.; Reichman, D. R. Path integral approach to the Wigner representation of canonical density operators for discrete systems coupled to harmonic baths. *J. Chem. Phys.* **2017**, *146*, 146.
(24) Makri, N. Improved Feynman propagators on a grid and non-adiabatic corrections within the path integral framework. *Chem. Phys. Lett.* **1992**, *193*, 435−444.
(25) Husimi, K. Some formal properties of the density matrix. *P. Phys. Math. Soc. Jpn.* **1940**, *22*, 264.
(26) Makri, N.; Miller, W. H. Coherent state semiclassical initial value representation for the Boltzmann operator in thermal correlation functions. *J. Chem. Phys.* **2002**, *116*, 9207−9212.
(27) Makri, N. Monte Carlo evaluation of forward-backward semiclassical correlation functions with a quantized coherent state density. *J. Phys. Chem. B* **2002**, *106*, 8390−8398.
(28) Voros, A. Wentzel-Kramers-Brillouin method in the Bergmann representation. *Phys. Rev. A: At., Mol., Opt. Phys.* **1989**, *40*, 6814−6825.
(29) Makri, N. Information guided noise reduction for Monte Carlo integration of oscillatory functions. *Chem. Phys. Lett.* **2004**, *400*, 446−452.
(30) Trotter, M. F. On the product of semi-groups of operators. *Proc. Am. Math. Soc.* **1959**, *10*, 545−551.
(31) Feynman, R. P. Space-time approach to non-relativistic quantum mechanics. *Rev. Mod. Phys.* **1948**, *20*, 367−387.
(32) Feynman, R. P. *Statistical Mechanics*; Addison-Wesley: Redwood City, 1972.
(33) Chandler, D.; Wolynes, P. G. Exploiting the isomorphism between quantum theory and the classical statistical mechanics of polyatomic fluids. *J. Chem. Phys.* **1981**, *74*, 4078−4095.
(34) Thoss, M.; Wang, H.; Miller, W. H. Generalized forward-backward initial value representation for the calculation of correlation functions in complex systems. *J. Chem. Phys.* **2001**, *114*, 9220−9235.
(35) Shao, J.; Makri, N. Forward-backward semiclassical dynamics without prefactors. *J. Phys. Chem. A* **1999**, *103*, 7753−7756.
(36) Shao, J.; Makri, N. Forward-backward semiclassical dynamics with linear scaling. *J. Phys. Chem. A* **1999**, *103*, 9479−9486.
(37) Jezek, E.; Makri, N. Finite temperature correlation functions via forward-backward semiclassical dynamics. *J. Phys. Chem. A* **2001**, *105*, 2851−2857.
(38) Metropolis, N.; Rosenbluth, A. W.; Rosenbluth, M. N.; Teller, H.; Teller, E. Equation of state calculations by fast computing machines. *J. Chem. Phys.* **1953**, *21*, 1087−1092.
(39) Liu, J.; Makri, N. Symmetries and detailed balance in forward-backward semiclassical dynamics. *Chem. Phys.* **2006**, *322*, 23−29.
(40) Chen, J.; Makri, N. Forward-backward semiclassical dynamics with single-bead coherent state density. *Mol. Phys.* **2008**, *106*, 443.
(41) Bukhman, E.; Makri, N. Forward-Backward Semiclassical Dynamics with Information-Guided Noise Reduction for a Molecule in Solution. *J. Phys. Chem. A* **2007**, *111*, 11320−11327.
(42) Chen, J.; Makri, N. Low-temperature correlation functions via forward-backward quantum dynamics. *Chem. Phys.* **2010**, *370*, 15−19.
(43) Caldeira, A. O.; Leggett, A. J. Path integral approach to quantum Brownian motion. *Phys. A* **1983**, *121*, 587−616.
(44) Makri, N. The linear response approximation and its lowest order corrections: an influence functional approach. *J. Phys. Chem. B* **1999**, *103*, 2823−2829.
(45) Walters, P. L.; Allen, T. C.; Makri, N. Direct determination of harmonic bath parameters from molecular dynamics simulations. *J. Comput. Chem.* **2017**, *38*, 110−115.
(46) Frisch, M. J.; Trucks, G. W.; Schlegel, H. B.; Scuseria, G. E.; Robb, M. A.; Cheeseman, J. R.; Scalmani, G.; Barone, V.; Mennucci, B.; Petersson, G. A.; Nakatsuji, H.; Caricato, M.; Li, X.; Hratchian, H. P.; Izmaylov, A. F.; Bloino, J.; Zheng, G.; Sonnenberg, J. L.; Hada, M.; Ehara, M.; Toyota, K.; Fukuda, R.; Hasegawa, J.; Ishida, M.; Nakajima, T.; Honda, Y.; Kitao, O.; Nakai, H.; Vreven, T.; J. A. Montgomery, J.; Peralta, J. E.; Ogliaro, F.; Bearpark, M.; Heyd, J. J.; Brothers, E.; Kudin, K. N.; Staroverov, V. N.; Kobayashi, R.; Normand, J.; Raghavachari, K.; Rendell, A.; Burant, J. C.; Iyengar, S. S.; Tomasi, J.; Cossi, M.; Rega, N.; Millam, J. M.; Klene, M.; Knox, J. E.; Cross, J. B.; Bakken, V.; Adamo, C.; Jaramillo, J.; Gomperts, R.; Stratmann, R. E.; Yazyev, O.; Austin, A. J.; Cammi, R.; Pomelli, C.; Ochterski, J. W.; Martin, R. L.; Morokuma, K.; Zakrzewski, V. G.; Voth, G. A.; Salvador, P.; Dannenberg, J. J.; Dapprich, S.; Daniels, A. D.; Farkas, O.; Foresman, J. B.; Ortiz, J. V.; Cioslowski, J.; Fox, D. J. *Gaussian 09*, A.01; Gaussian, Inc.: Wallingford, 2009.
(47) Dunning, T. H. Gaussian basis sets for use in correlated molecular calculations. I. The atoms boron through neon and hydrogen. *J. Chem. Phys.* **1989**, *90*, 1007.
(48) Woon, D. E.; Dunning, T. H. Gaussian basis sets for use in correlated molecular calculations. V. Core-valence basis sets for boron through neon. *J. Chem. Phys.* **1995**, *103*, 4572.
(49) Ceperley, D. M. Path integrals in the theory of condensed helium. *Rev. Mod. Phys.* **1995**, *67*, 279−355.

DOI: 10.1021/acs.jpca.9b00758
J. Phys. Chem. A 2019, 123, 4284−4294